Nematic-like elastic coefficients of the SmA b phase

Claire Meyer, Patrick Davidson, Tatiana Sergan, Vassili Sergan, Daniel Stoenescu, Anamarija Knežević, Irena Dokli, Andreja Lesac, Ivan Dozov

Nematic-like elastic coefficients of the SmA_b phase

Claire Meyer[1*], Patrick Davidson[2], Tatiana Sergan[3], Vassili Sergan[3], Daniel Stoenescu[4], Anamarija Knežević[5], Irena Dokli[5], Andreja Lesac[5] and Ivan Dozov[1,2]

[1]Physique des Systèmes Complexes, Université de Picardie Jules Verne, 80039 Amiens, France
[2] Laboratoire de Physique des Solides, Université Paris-Saclay, CNRS, 91405 Orsay, France
[3]California State University, Sacramento, 6000 J Street, Sacramento, California 95608, USA
[4]Optics Department, IMT Atlantique, CS 83818, 29238 Brest cedex, France
[5]Ruđer Bošković Institute, Bijenička 54, 10000 Zagreb, Croatia

ABSTRACT: The synthesis of bent-shaped mesogens and mesogenic dimers has renewed the field of liquid crystals in many ways during the previous decades, for example through the discovery of "exotic" mesophases such as the twist-bend nematic phase and the biaxial SmA phase (SmA_b). Recently, we reported on the observation of a SmA_b with a bent-shaped dimer, and on its fast electro-optic effect that we interpreted as a biaxial Fréedericksz transition (BFrTr) of the secondary **m**-director under applied electric field (C. Meyer et al, Phys. Rev. X, **11**, 031012 (2021)). In this study we used dielectric and birefringence techniques to directly measure the splay, K_{11}^m, and bend, K_{33}^m, elastic constants that characterize the elastic distortion modes of the **m**-director. We observed that during the BFrTr, domains of opposite tilt appear and are often enclosed in elliptical defect loops, just like those observed during the usual Fréedericksz transition of common nematics, which allowed us to obtain the third (twist) elastic constant K_{22}^m, from the defect loop ellipticity. Although K_{11}^m and K_{33}^m are of the same order of magnitude as K_{11} and K_{33} in the nematic phase of bent-shaped dimers, K_{22}^m is an order of magnitude smaller than K_{11}^m and K_{33}^m and also than K_{22} of 5CB. We argue that these features could be generic for the intercalated SmA_b phase of bent-shaped dimers.

I. INTRODUCTION

The nematic phase (N) is the most simple and best studied liquid-crystal (LC) phase. It is a uniaxial anisotropic fluid with long-range orientational order and no long-range positional order. The rod-like molecules of the nematic are oriented with their long axes preferentially parallel (or antiparallel) to the nematic director, **n**, which is along the $D_{\infty h}$ symmetry axis of the phase. In the ground state, the director field is uniform, and its distortion requires an elastic energy given by [1]:

$$f^n = \frac{1}{2}\left[K_{11}\left(\mathbf{n}(\boldsymbol{\nabla}\cdot\mathbf{n})\right)^2 + K_{22}\left(\mathbf{n}\cdot(\boldsymbol{\nabla}\times\mathbf{n})\right)^2 + K_{33}\left(\mathbf{n}\times(\boldsymbol{\nabla}\times\mathbf{n})\right)^2\right], \quad (1)$$

where the vectors $\mathbf{n}(\boldsymbol{\nabla}\cdot\mathbf{n})$ and $\mathbf{n}\times(\boldsymbol{\nabla}\times\mathbf{n})$ and the pseudo-scalar $\mathbf{n}\cdot(\boldsymbol{\nabla}\times\mathbf{n})$ describe, respectively, the splay, bend, and twist distortions of the director **n**, and K_{11}, K_{33}, and K_{22} are the respective elastic moduli.

The distortion elasticity of the nematic phase plays an important role for its ubiquitous technological applications, which are based on the competition between the torques applied to the director by the surface alignment and by the applied electric field. A typical example is when a voltage U is applied to a nematic with positive dielectric anisotropy, $\Delta\varepsilon > 0$, in a uniformly aligned planar cell (**n** parallel to the surfaces). Up to some threshold voltage U_c, the director remains uniform as the electric torque is too weak to distort the nematic. However, for $U > U_c$, the director is distorted in the bulk of the cell while remaining planarly oriented at the two boundary surfaces (see Appendix A). This field-induced effect [2, 3] is known as the Fréedericksz transition (FrTr) and it is one of the most important electrooptic effects in the nematic phase as it is the basis of most of the display applications of liquid crystals.

Different and less symmetric nematic phases are obtained when the shape of the mesogenic molecules significantly differs from rod-like. For example, bent-shaped molecules form a nematic phase with spontaneously broken chiral symmetry that is called the twist-bend nematic, N_{TB} [4, 5]. Another phase, the splay-bend nematic, N_{SB}, has also been predicted [4, 6] for bent-shaped molecules but still remains elusive. These two modulated nematic phases present elastic properties that are different from those of the usual uniaxial N-phase. They show strong spontaneous bend distortion, which has been explained with a negative value of the bend modulus, $K_{33} < 0$, either plain [4] or renormalized by the flexoelectric effect [6].

Strongly biaxial molecules, e.g. board-like, have been predicted long ago [7] to form biaxial nematic (N_b) phases. The orientational order of this phase is biaxial: the long molecular axis is still, on average, parallel to the primary director **n**, but the medium axis of the molecules (along their width) is, on average, parallel to a secondary director **m**, **m** $\perp$ **n**. The N_b phase has been reported for lyotropic systems [8] but its existence for thermotropic nematics is still actively debated [9]. Due to the lower symmetry of the N_b phase (D_{2h}), its elasticity is expected to be quite different from that of usual nematics. Indeed, twelve distinct elastic moduli are needed [10, 11] to describe all the distortion modes for both, **n** and **m** directors which promises a very rich behavior of the field-induced textural transitions in the N_b phase.

Smectic (Sm) phases form another large class of LCs. They have not only long-range orientational order like nematics but also long-range positional order because the molecules form stacks of equidistant smectic layers. The simplest Sm phase is the smectic A (SmA). In this phase, the director **n** is parallel to the normal to the layers, i.e. to the wave vector **q** of the smectic density wave. Therefore, the SmA is uniaxial, with the same $D_{\infty h}$ symmetry as the N phase. However, the elastic energy of the SmA is different from the nematic case: in addition to the energy involved in distortions of the director field, which is similar to that in Eq. (1), there are additional terms related to the compression and/or dilation of the layers, and to the tilt of **n** away from **q**. The elastic energy corresponding to these specific smectic terms is much higher than the one related to the **n** distortion. Moreover, due to the incompatibility of the bend and twist distortions of the director **n** with the layered smectic structure, these modes are practically forbidden in SmA and therefore only the splay remains possible. As a consequence, the Fréedericksz transition is impossible in SmA because the tilt of **n** away from **q** requires a huge elastic energy. Instead, under strong fields, the SmA undergoes the so-called "ghost transitions" [3, 12] with the amplitude of the tilt of **n** so small that they are difficult to observe.

When the mesogenic molecules of nematics are board-like or strongly bent-shaped [13, 14, 15], they can form biaxial smectic A (SmA_b) phases in addition to the N-phase. As in the N_b case, there are two distinct directors in the SmA_b: the primary director, **n**, that is parallel to the layer normal and defines the average orientation of the long molecular axis, and the secondary director, **m**, that is parallel to the smectic layer and defines the average orientation of the medium molecular axis. Since the symmetry of the SmA_b is the same as that of the N_b phase (D_{2h}), its elastic energy is expected to be very complicated,

with twelve nematic-like terms that describe the distortion of the two directors and smectic-like terms that describe the compression of the layers and the tilt of **n** with respect to **q**.

Recently, studying the electrooptic effects in a SmA_b phase formed by bent-shaped mesogenic dimers [16], we demonstrated that, under realistically strong electric fields, the elastic behavior of the SmA_b is in fact much simpler than that of the biaxial nematic. Indeed, the smectic terms in the elastic energy forbid the bend and twist of the primary director because these distortions are incompatible with the condition **n** || **q** and thus require a huge smectic distortion energy. Even the splay distortion of **n** is energetically very costly in confined geometry because it requires reorganization of the layers. Therefore, as long as the layered structure remains unperturbed, the only possible distortions must be related to the **m**-director because its rotation in the plane of the layers does not alter the periodic structure, and, therefore, costs no smectic distortion energy.

In our previous work [16] we studied the electro-optical properties of a LC mixture that was primarily made of bent-shaped molecular dimers consisting of two identical monomers connected by a $(CH_2)_7$ aliphatic chain, with their long axes tilted towards each other at ~118° angle at apex [17] (Fig. 1a). This mixture shows a SmA_b phase with the monomers arranged in smectic layers; the thickness of each layer is about one-half of the molecular length in its lowest-energy conformation. The layers are intercalated so that each dimer spans two neighboring layers, with their long molecular axes l aligned along the normal to the smectic layer **q**. The sign of the tilt angle of the monomer axis alternates layer-to-layer so that a cross-sectional view of the structure looks like books on bookshelves with their spines tilted in alternating directions (Fig. 1b).

Such a structure is optically biaxial, and can be characterized by an ellipsoid of the wave normals (optical indicatrix or index ellipsoid) that has three different semi-axes of length n_{nn}, n_{mm}, and n_{kk}, with the n_{nn} axis along the long molecular axes and perpendicular to the smectic layers, and the n_{mm} axis parallel to the smectic layer. The primary director **n** coincides with the n_{nn} axis of the indicatrix. The secondary director **m** is associated with the projection of the monomer axes on the plane of the smectic layers and is along the n_{mm} axis of the indicatrix (Fig. 2).

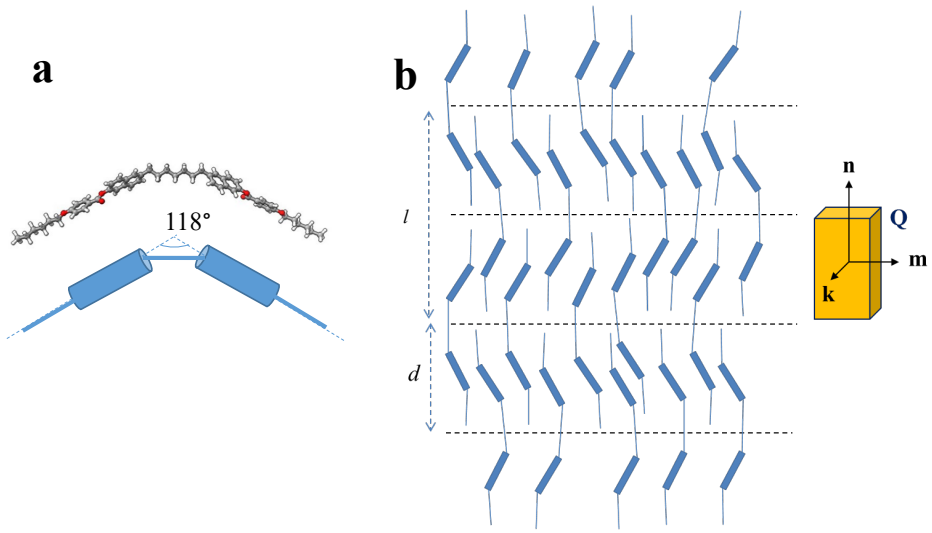

Fig. 1 : Schematic representation **(a)** of the dimer 1,7-Bis(6-(4- hexyloxybenzoyloxy) naphthalene-2-yl) heptane (BNA-76) and of the structure of the intercalated SmA_b phase **(b).** The dimer molecules of length *l* are perpendicular to the completely intercalated smectic layers. The period of the structure, i.e. the layer thickness, is $d \approx l/2$. In each layer, the monomers are tilted, as in a SmC, and the sign of the tilt alternates from one layer to the next. The order parameter tensor of the dimers, **Q**, represented as a parallelepiped, is biaxial. The primary director, **n**, is perpendicular to the layers and any deviation from this direction requires a huge smectic energy. The secondary director, **m**, is parallel to the layer and the monomers are preferentially aligned parallel to the **mn**-plane. In the ground state of the phase, **m** is uniform, and its in-plane orientation is degenerated. The distortion of **m** requires only a nematic-like energy, in exact analogy with the **n**-distortions in the nematic phase.

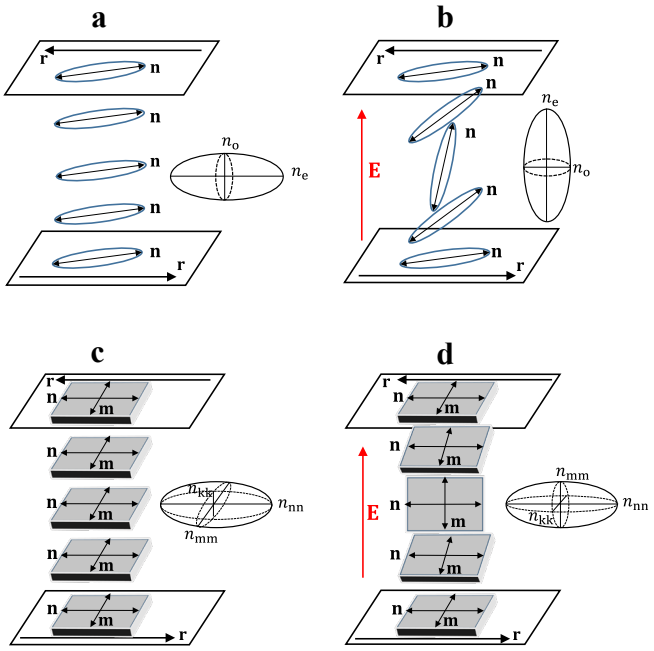

Figure 2. Representations of the molecular alignment and the indicatrix in a planar cell in the case of rod-shaped molecules in the absence of applied voltage (**a**) and in an external electric field **E** (**b**) and of board-like molecules in the absence of applied voltage (**c**) and in an external electric field **E** (**d**). (For simplicity, the pretilt of the **n**-director is not represented in **c** and **d**.)

The birefringence properties of the SmA_b phase were studied in planar cells filled with the LC mixture at the isotropic-phase temperature and then cooled to the nematic phase. Cooling resulted in a uniform planar alignment, with the nematic director **n** along the rubbing direction **r**. Further cooling resulted in the formation of large monochiral

N_{TB} domains with their optic axes along **r** and alternating handedness of chirality. Further cooling led to the coexistence of N_{TB} and SmA_b domains, and then, eventually, to the formation of SmA_b domains that were large enough to allow for the measurement of the local optical retardation of the cell, ΔL. Analysis of the textures under a polarizing microscope supported the alignment of the primary director **n** and, hence the n_{nn} axis, along **r** and along the helix of the N_{TB} domains; the smectic layers of the SmA_b domains were perpendicular to **n**. The secondary director **m** and the n_{mm} axis of the indicatrix were found to be in the plane of the cell, parallel to the smectic layer, and perpendicular to the primary director **n**. Thus, without electric field, the optical retardation of the cell, ΔL, was determined by the difference n_{nn} - n_{mm}. Heating the sample to the isotropic phase and then cooling it back to the SmA_b phase in the presence of a strong electric field aligned the primary director **n** along the normal to the cell, with the smectic layers parallel to the cell substrates. This allowed us to demonstrate the biaxiality of the SmA_b phase and we have shown that the difference n_{mm} - n_{kk}, although small, is nevertheless significant.

Locking of the primary director **n** in the SmA_b phase along the rubbing direction **r** in planar cells allows for an independent rotation of the secondary director **m** in the external electric field. This process takes place without altering the layered structure, and implies the possibility of a biaxial Fréedericksz transition (BFrTr), which was confirmed experimentally [16], and is illustrated in Fig. 2. When a voltage U was applied to the planar cells, with the electric field **E** perpendicular to the cell, the optical retardation of the SmA_b domains increased due to the rotation of the secondary director **m** about the fixed primary director **n**. The increase of the optical retardation is consistent with $n_{mm} > n_{kk}$ since, in the presence of the field, the optical retardation is determined by $(n_{nn} - n_{eff})$ which is larger than $(n_{nn} - n_{mm})$, where $n_{eff} = \frac{n_{mm} n_{kk}}{\sqrt{n_{mm}^2 \cos^2\theta + n_{kk}^2 \sin^2\theta}}$ and $\theta = \theta(U)$ is the angle between **m** and **E**. The threshold voltage of this BFrTr, $U_c^m \sim 4$ V, is less than twice the value measured in the nematic phase of the same compound for the classical FrTr, while the field-off relaxation time is about 30 times faster. These features make the BFrTr very attractive for technological applications.

Decoupling **m** from **n** in the planar SmA_b domains allows for the description of its elasticity with the help of a nematic-like distortion energy [16]:

$$f^m = 1/2\,\{K_{11}^m\,[\mathbf{m}(\boldsymbol{\nabla}\cdot\mathbf{m})]^2 + K_{22}^m\,[\mathbf{m}\cdot(\boldsymbol{\nabla}\times\mathbf{m})]^2 + K_{33}^m\,[\mathbf{m}\times(\boldsymbol{\nabla}\times\mathbf{m})]^2\}\,, \qquad (2)$$

which is a direct analogy of the usual uniaxial nematic elastic energy but involves only the distortions of the **m**-director. Here K_{ii}^{m}, for i =1,2,3, are the elastic moduli for splay, twist, and bend distortions of **m**, respectively [16].

By accurately measuring the dependence of the capacitance on the voltage applied to the cells, *C(U)*, and then fitting it with a theoretical model [18, 19], we estimated the values of the K_{11}^{m} and K_{33}^{m} moduli in the SmA_b phase and found them slightly lower than the corresponding values measured in the nematic phase for the **n**-director distortions. However, K_{22}^{m} cannot be measured in this way because the twist distortion is not involved in the BFrTr transition. Also, these dielectric measurements cannot be applied to any of the K_{ii}^{m} within the wide (~5°C) coexistence range of the SmA_b and N_{TB} phases because such measurements would require a large monophasic domain [16]. In this work, we use a different technique to analyze the BFrTr that allows for the measurement of all three K_{ii}^{m} constants in the SmA_b phase as well as in the SmA_b - N_{TB} biphasic coexistence range. Our results show that the anisotropy of the biaxial nematic-like elastic constants in the SmA_b phase, $K_{11}^{m} > K_{33}^{m} >> K_{22}^{m}$, is very unusual compared to that of the uniaxial nematic phase of typical rod-like mesogens or even to that measured in the nematic phase of the same BP12 mixture.

II. MATERIALS AND METHODS

A. Liquid crystal materials.

For this work, we used the LC mixture "BP12" consisting of 88% (by weight) of 1,7-Bis(6-(4-hexyloxybenzoyloxy)naphthalene-2-yl)heptane dimer (BNA-76) (Fig. 1) [17] and 12% of the rod-like nematogen 4′-cyano[1,1′-biphenyl]-4-yl 4-hexylbenzoate (6-PEPP-N) (commercially available from Xi'an Ruilian, China) (Fig. 3) [16]. The phase transition temperatures of the mixture measured by DSC are: Iso – 162 °C - N - 109 °C - N_{TB} - 102 °C - N_{TB}/SmA_b - 97 °C - SmA_b - ~ 70 °C - Cr

Note that the BP12 mixture has an unusually wide (≈ 5°C) temperature range of coexistence of the N_{TB} and SmA_b phases.

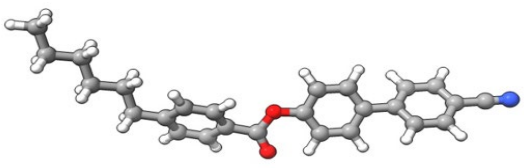

Figure 3. Schematic representation of 4′-cyano[1,1′-biphenyl]-4-yl 4-hexylbenzoate (6-PEPP-N)

B. Sample preparation

In our experiments we used planar cells assembled with anti-parallel rubbing directions of polyimide alignment layers deposited on the conducting layers serving as electrodes which allowed us to apply the electric field normal to the cell substrates. Depending on the task, we used cells with different gaps. The thinner cells with a gap of about 1.5 μm showed faster relaxation of the **m** director during the transition and thus were used for the birefringence study of the BFrTr. Cells with gaps of 5 and 9.8 μm were used for the studies of the shape of the domain walls under electric field because the thicker cells provided for slower collapse of the domain-wall loops. The cells were filled by capillarity with the BP12 mixture in the isotropic phase and were then slowly cooled down. The alignment layers provide a pretilt angle of 2° for the **n** director in the nematic phase and about zero pretilt for both **n** and **m** in the SmA_b phase. Large monophasic planarly-aligned single domains of the SmA_b phase suitable for the dielectric and birefringence investigation of the BFrTr were obtained by applying thermal and electric field oscillations during the slow cooling of the cells through the N_{TB} and N_{TB}/SmA_b temperature range, as described previously [16]. The zero-pretilt of **m** in the SmA_b phase allowed for the appearance of "twin" domains (domains with opposite directions of director tilt in the middle of the cell) above the BFrTr threshold that were required for the measurement of the K_{22}^m elastic modulus.

C. Dielectric measurements

We used the same dielectric technique and measuring setup that were described in [16]. The technique is based on the measurement of the cell capacity $C(U)$ (10-μm-thick commercial cells (MUT, Poland) treated to provide planar alignment) under increasing applied voltage U. This gives the values of the dielectric tensor components $\varepsilon_\perp = \varepsilon_{kk}$ and $\varepsilon_\parallel = \varepsilon_{mm}$, with the **m**-director perpendicular and parallel to the applied field at $U = 0$ and high voltage, respectively. Fitting of the $C(U)$ curve with the results of simulations based on the well-established theory of the FrTr in nematics [16, 20, 21, 22] provides the value of the Fréedericksz threshold voltage U_c^m and the splay elastic constant K_{11}^m. The slope of the BC part of the $C(U)$ curve in Figure 10 depends on the ratio K_{33}^m / K_{11}^m, and thus provides the value of K_{33}^m.

This technique allows for almost complete characterization of the nematic-like elasticity of the SmA_b phase with an important exception of the twist elastic constant K_{22}^m that cannot be measured due to the difficulty in obtaining the cell geometry required for the twist FrTr. Another limitation of this technique is the requirement of a monophasic region spanning the whole area between the cell electrodes because the capacitive signal is integrated over the electrode area. Therefore, the wide biphasic temperature range is inaccessible for this technique. This limitation is an important drawback for the BP12 case, as the variation of the elastic constants can be significant in this range due to the fast variation of the in-layer orientational order close to the N_{TB}/SmA_b phase transition.

D. Birefringence measurements.

To measure the elastic constants in the biphasic region, we use a birefringence measurement technique inspired by previous works for the nematic phase [20, 22]. Indeed, the birefringence measurement is local, and can be performed with excellent precision within a uniform domain with size as small as 10 × 10 μm^2. The details of the measurement technique and setup are published in [16, 23]. In brief, we measure the voltage dependence of the optical path difference at normal incidence, $\Delta L(U) = L_{\parallel} - L_{\perp}$, where $L_{\parallel}$ and $L_{\perp}$ refer to the optical paths for light polarized parallel and perpendicular to the primary director **n**, respectively, in a thin (1.5 μm thick) cell with planar alignment. $\Delta L(U)$ is measured under polarizing microscope (Leitz Ortholux) equipped with a Sénarmont compensator and a highly sensitive photomultiplier-based photometer. Our optical measurement system has a small window with a variable size of about 20 μm × 20 μm. By adjusting its position and size, we could acquire the signal from a uniform single SmA_b domain and thus measure $\Delta L(U)$ in the N_{TB}-SmA_b co-existence temperature range. $\Delta L(U)$ can be expressed [16] in terms of the three refractive indices of the biaxial phase, n_{nn}, n_{mm}, and n_{kk}:

$$\Delta L(U) = \int_0^d \left[n_{nn} - \frac{n_{mm} n_{kk}}{\sqrt{{n_{mm}}^2 \cos^2\theta + {n_{kk}}^2 \sin^2\theta}} \right] dz, \qquad (3)$$

where θ is the angle between **m** and the normal to the cell.

The fitting of the $\Delta L(U)$ curve with the theoretical model provides precise values for the BFrTr threshold, U_c^m, and n_{nn} - n_{mm} and $n_{nn} - n_{kk}$. Moreover, if the dielectric tensor components ε_{mm} and ε_{kk} are

available from another experiment, the fit provides, by analogy with the dielectric case, the values of K_{11}^m and K_{33}^m.

E. Measurement of K_{22}^m by fitting the shape of the domain-wall loops

For the measurement of the elastic constant K_{22}^m, we used a technique that was proposed long ago for nematics in the zero-pretilt cell geometry [24] and was shown to give reliable values of a ratio of elastic constants [25, 26]. It is based on the analysis of the shape of the domain walls separating two types of domains with opposite director tilt angles that occur in the bulk of the nematic layer during the FrTr. The textures of the two domains are symmetric (see Fig. 4) and hence have the same total energy. When a high enough voltage is applied abruptly in a zero-pretilt nematic cell, the mass-flow generated by the fast rotation of the director favors the formation of two types of domains, so-called "twin-domains", that are separated by characteristic domain walls (DWs). Because the director tilt angle changes sign inside the domain wall, the elastic energy of the wall is higher than that in the twin-domains. Therefore, the wall costs some excess energy per unit surface that depends on the wall orientation. When the DW forms a closed loop around a uniform domain of one type, the loop starts shrinking progressively under its line tension (the line tension is the excess energy of the wall integrated over the cell thickness), and eventually disappears. In order to minimize its total energy, the loop keeps its equilibrium shape during contraction since it is defined only by the anisotropy of the line tension.

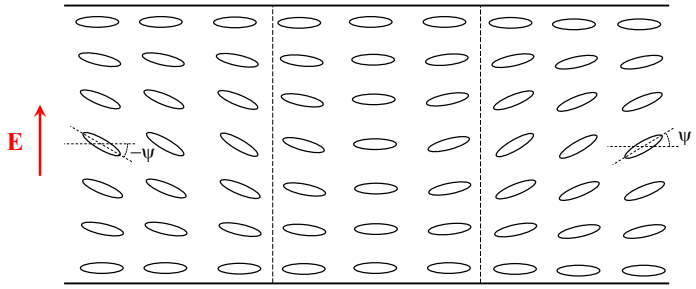

Figure 4. FrTr in a nematic cell with two twin domains (on the left and right) separated by a wall (the region in the middle, between the vertical dashed lines). In the two domains, the tilt angles of the director with respect to the cell surfaces have opposite signs and the tilt vanishes in the middle of the wall.

Originally, this technique was proposed by F. Brochard [24] who considered the case of a magnetic field-induced FrTr in a planar cell. In her theoretical treatment, she adopted the two-constant approximation: $K_{11} = K_{33} = K \neq K_{22}$. Under this assumption, the quasi-equilibrium shape of the loop was predicted to be an ellipse, with the ratio of its axes $a_{\parallel} / a_{\perp} = (K/K_{22})^{1/2}$ (here the subscripts refer to the orientation of the long axis of the ellipse with respect to the preferred director orientation at the cell surface). Experiments conducted by L. Leger [25, 26] confirmed this prediction and demonstrated that this technique is reliable for the measurement of the ratio of elastic constants.

Because of the similarity between the distortion energies of the uniaxial nematic (associated with re-orientation of **n**) and biaxial SmA_b (associated with the decoupling and independent rotation of **m** about the strongly anchored **n**), we expect that the same technique can be applied for the BFrTr in the SmA_b phase. However, in this case, the approach needs to be generalized to an electric field-induced FrTr, which is more complex because the field in the sample is not uniform due to the finite and non-negligible value of $\Delta\varepsilon/\varepsilon_{\perp}$ [27]. Moreover, due to the significant difference between the values of K_{11}^m and K_{33}^m for our material, we need to consider the complete anisotropy of the elastic moduli, $K_{11} \neq K_{22} \neq K_{33}$. The generalized treatment performed for the case of a usual nematic is presented in Appendixes A and B. Remarkably, despite the significant difference in the absolute value of the excess energy of the wall compared to the simpler case described in Ref. [24], the shape of the loop in quasi-equilibrium is also an ellipse, with axial ratio $a_{\parallel} / a_{\perp} = (K_{33}/K_{22})^{1/2}$. Thanks to the analogy between the FrTr in the nematic and BFrTr in the SmA_b phases, we obtain for the SmA_b case:

$$a_{\parallel}^m / a_{\perp}^m = (K_{33}^m / K_{22}^m)^{1/2}, \qquad (4)$$

where the subscripts refer to the orientation of the ellipse axes with respect to the director **m** in the absence of field. A typical case of a loop around one of the twin domains during the BFrTr is shown in Fig. 5. The shape of the loop is indeed elliptical, with its major axis parallel to the **m**-director and an axial ratio of about 3, which suggests an unusually high value of the K_{33}^m/K_{22}^m ratio.

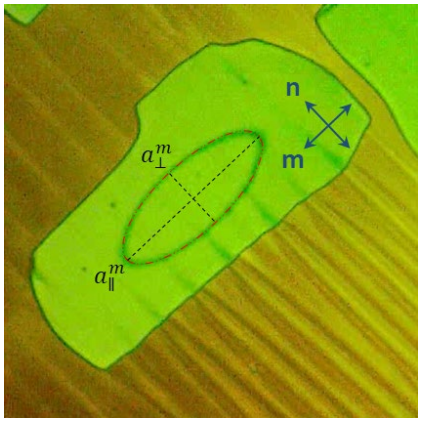

Figure 5. Biphasic SmA_b/N_{TB} sample at T = 102.0 °C under electric field ($U = 5$ V $> U_c^m$, $f = 6$ kHz). The BFrTr takes place in the SmA_b regions (green). The blue double-headed arrows show the orientation of the **n**- and **m**-directors of the SmA_b phase. The elliptically shaped DW that separates one of the twin domains from the other is clearly

visible in the SmA_b region (dark line). The dashed red line that is superposed on the wall is an ellipse with axial ratio $a_{\parallel}^{m}/a_{\perp}^{m} = 2.66$.

To induce the formation of the domain-wall loops, we abruptly apply a d.c. or a.c. ($f = 6$ kHz, $U = 5$ V_{rms}) voltage (Fig. 6). Similarly to the nematic case [3], the fast rotation of **m** under the applied electric field induces backflow and the formation of electro-convective rolls, which results in the emergence of both kinds of twin-domains separated by DWs. At first, the domain walls are irregular, with curvature at all possible wave lengths (Fig. 6 b). However, due to the high line-tension, the DWs start shrinking and, gradually, the loops relax to an elliptical shape (Fig. 6 d). Then, the loops further slowly shrink due to the line tension. In this process, their axial ratio remains approximately constant (the plateau region in Fig. 7). Such behavior is a signature of a quasi-equilibrium process. Finally, at the end of the process, the loop contraction rate increases until the domains vanish. In this out-of-equilibrium regime, the axial ratio starts varying (a low-value outlier in Figure 7). To precisely measure the time dependence of the axial ratio as the domains collapse, we recorded videos of the process, and then analyzed them frame-by-frame. Only sequences for which the axial ratio remains constant were used for further analysis because they correspond to a quasi-equilibrium regime for which Eq. (4) is valid. (Some other sequences demonstrate a different behavior, mainly due to the pinning of the walls on surface defects or on the N_{TB}/SmA_b interface.)

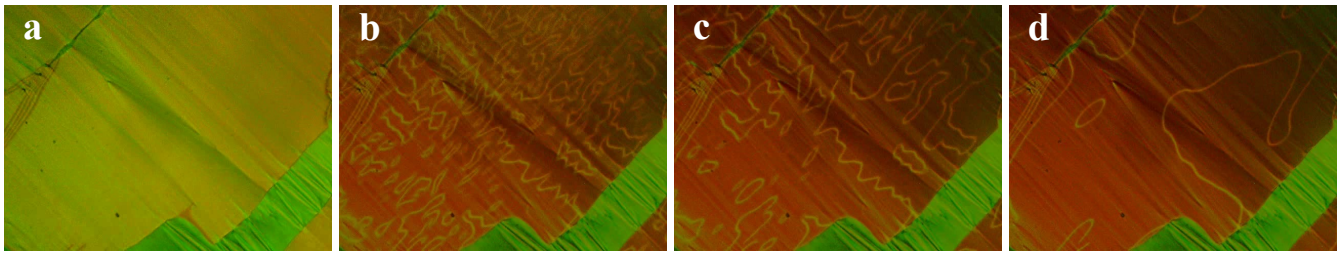

Figure 6. Formation of twin domains and coarsening of the domain structure (98 °C). The green regions are in the N_{TB} phase, the brown regions are the twin domains in the SmA_b phase under field ($U = 9$ V, $f = 6$ kHz), the yellow regions correspond to planar orientation either at $U = 0$ (**a**) or within the domain walls (**b-d**). The photos were taken before (**a**) and 0.03, 0.06 and 0.45 seconds after turning on the electric field (**b-d**), respectively.

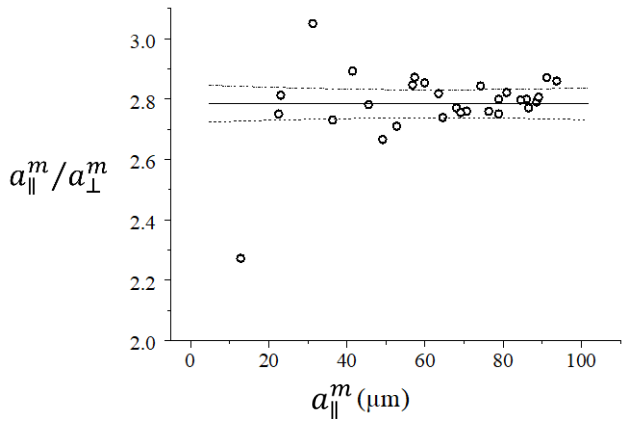

Figure 7. Evolution of the axial ratio of the elliptical loops. When the loop is in quasi-equilibrium in absence of pinning on the surfaces and of defects of the texture, it shrinks keeping its axial ratio almost constant (open symbols, 102.3 °C). The solid line shows the average value of the plateau and the dashed lines show the upper and lower 95% confidence limits.

III. RESULTS AND DISCUSSION

A. Dielectric and elastic properties obtained by fitting the *C(U)* curve

C(U) curves were measured at different temperatures (see Section II) and fitted with the theoretical models. The multi-step fitting procedure is non-trivial, and was performed for each temperature as follows:

1. First, ε_{kk} was determined and ε_{mm} was estimated from the capacitance and appropriate cell geometry at low and high voltages respectively. The third component, ε_{nn}, was measured in a field-induced quasi-homeotropic domain as described in [16];
2. A rough estimation of the value of the Fréedericksz threshold voltage U_c^m and data from step 1 were used to calculate the splay elastic constant K_{11}^m;
3. The slope of the linear portion of the *C(U)* curve was used to estimate K_{33}^m/K_{11}^m ratio, and thus K_{33}^m itself;
4. The parameters found in steps 1-3 were used as initial conditions for the precise fitting procedure. The **m**-director distribution was calculated for each voltage (using Euler-Lagrange formalism) and was then used to calculate the theoretical *C(U)* curve. By varying the K_{11}^m, K_{33}^m, and ε_{mm} parameters, an almost perfect fit of the experimental *C(U)* curve can be obtained. This fitting procedure is multi-parametric, which raises the question of its uniqueness. However, as mentioned in the Section II, the various parts (A-E in Fig. 10) of the *C(U)* curve have different sensitivities to variations of different fitting parameters. For example: (i) the almost flat segments at the beginning (part AB) and the end (part DE) of the curve give the ε_{kk} and ε_{mm} values respectively; (ii) the voltage at which the capacity starts increasing rapidly gives the approximate value of U_c^m, and is very sensitive to K_{11}^m; (iii) the curvature at point B is mostly defined by the

pretilt; (iv) the slope of the segment BC is sensitive to the K_{33}^m/K_{11}^m ratio. Thus, we believe that the dielectric and elastic constants obtained by our fitting procedure are accurate;

5. The procedure was repeated for various temperatures within the SmA_b range, and the results are presented in Fig. 8 and 9.

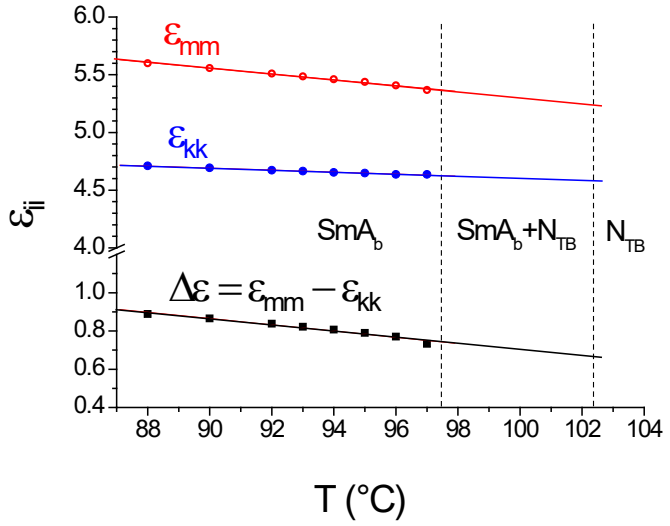

Figure 8. Temperature dependence of the dielectric tensor components measured in the SmA_b phase [16] and their extrapolation in the biphasic region.

It is impossible to measure the dielectric constants in the biphasic region using the method described above. The presence of N_{TB} domains leads to non-uniform response of the sample in an external electric field and, therefore, to incorrect values of ε_{kk} and ε_{mm}. However, the linear dependence on temperature of both ε_{kk} and ε_{mm} across the whole SmA_b range allows for its extrapolation in the biphasic region (Fig. 8).

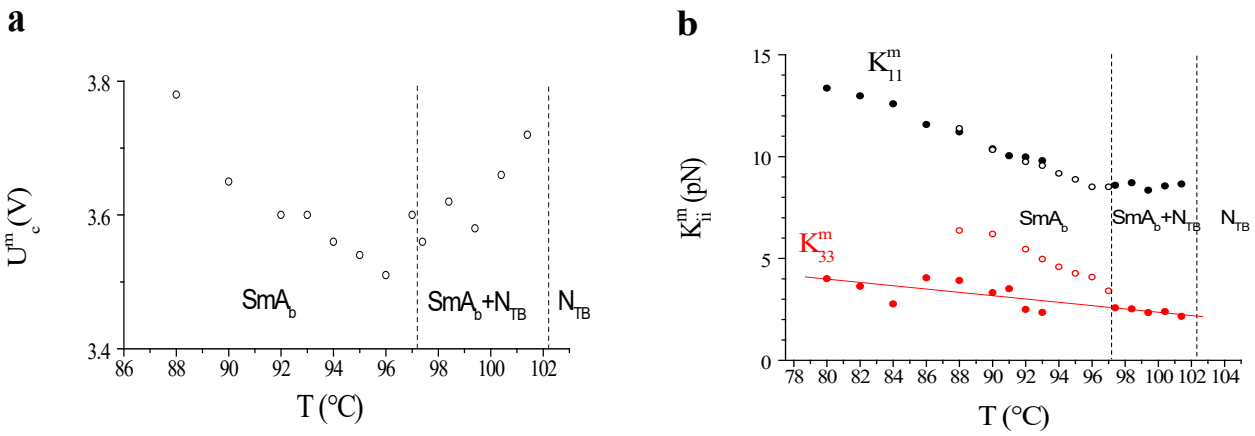

Figure 9. Temperature dependences of the Fréedericksz threshold U_c^m (**a**) and the elastic constants K_{11}^m and K_{33}^m (**b**) obtained by fitting the *C(U)* curves (in the monophasic SmA_b range of the BP12 mixture [16], open symbols) and the optical retardation (solid symbols, discussed below) with the theoretical model. The solid line is a linear interpolation of the K_{33}^m data used for calculation of K_{22}^m.

B. Elastic properties obtained from fitting the Δ*L*(*U*) curves

The fitting procedure of the Δ*L*(*U*) curves is almost identical to the one described in section III A. The only difference is that the initial fitting parameters are n_{kk}, n_{mm} (measured in [16]), and ε_{kk}, ε_{mm} (which are needed for the calculations of the **m**-director distribution and were determined in the previous section). The experimental Δ*n*(*U*) curve and the best fit for one of the temperatures within the SmA_b range are shown in Fig. 10 to illustrate the good quality of the fit. As mentioned above, fitting the Δ*L*(*U*) curve offers a significant advantage over dielectric methods, because it allows for the determination of K_{11}^m and K_{33}^m in the biphasic range of the BP12 mixture [16].

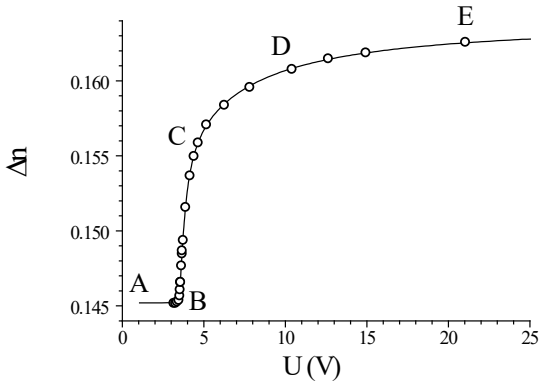

Figure 10. Voltage dependence of the birefringence measured in the SmA_b phase at $T = 93.0$ °C (open circles) and its best fit (solid line) by the theoretical model of the BFrTr.

The data for K_{11}^m and K_{33}^m in both the SmA_b and the biphasic range are presented in Fig.9 along with data obtained using the dielectric method.

C. Comparison of dielectric and optical methods

As evident from Fig. 9, the K_{11}^m values determined via the dielectric method are in excellent agreement with those determined by fitting the $\Delta L(U)$ curve, therefore, both methods appear to be reliable. The results for K_{33}^m, however, are significantly different: The values of K_{33}^m obtained by the dielectric method are considerably higher at all temperatures, although the discrepancy diminishes with increasing temperature. This discrepancy can be explained by analyzing the textural changes in the sample in the vicinity of U_c^m. Figure 11 shows microphotographs of a SmA_b sample at different applied voltages. The sample looks almost uniform with few defects at $U \leq U_c^m$ (Fig. 11 a), however, at $U \approx U_c^m$, many more defects appear in the field of view (Fig. 11 b). These defects are mostly walls that separate the twin-domains with opposite signs of the tilt angle. At low temperature, the walls are pinned to the surfaces and inhomogeneities of the texture. At higher voltages, some of the walls disappear due to the shrinkage of the loops but others remain as they are strongly pinned (Fig. 11 c). As long as the voltage remains higher than U_c^m, these strongly pinned defects do not disappear, and only their thickness decreases with increasing voltage.

Figure 11. SmA_b sample at T = 88.0 °C under electric field: **a**) $U = 3.09$ V_{rms}; **b**) $U = 4.24$ V_{rms}; **c**) $U = 4.80 V_{rms}$ ($f = 6$ kHz). The cell is observed under a polarizing microscope with a Senarmont

compensator for better visualization - darker state corresponds to higher birefringence. Scale bar: 100 µm.

Because the capacitance of the sample depends on the dielectric permittivity of the material averaged over the whole active area, the presence of areas with the director oriented differently from its orientation within the monodomain leads to a capacitance that is lower compared to that of a perfectly uniform texture. This affects very little the experimental value of U_c^m and, therefore, the calculated value of K_{11}^m. However, the presence of the defects alters the slope of *C(U)* in its steeper part (Fig. 12) which depends almost exclusively on K_{33}^m/K_{11}^m. Thus, with K_{11}^m essentially unaffected, the presence of the defects significantly affects the calculated value of K_{33}^m.

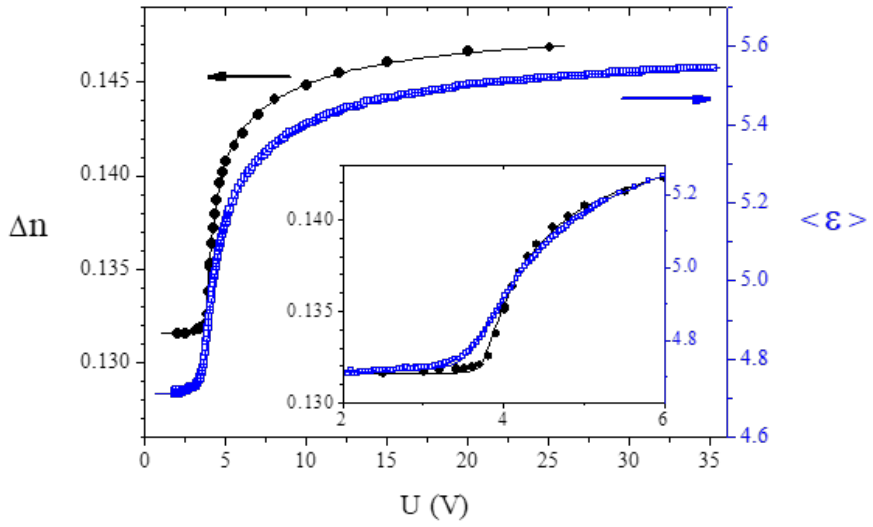

Figure12. Voltage dependence of the birefringence (left scale) and the average dielectric constant (right scale) in the SmA_b phase of the BP12 mixture at 88 °C. The symbols are the experimental results and the solid lines show the best fit with the theoretical model. The threshold voltages, U_c, computed from the two fits are respectively 3.89 and 3.78 V, resulting in almost identical values of the elastic constant K_{11}^m. On the contrary, the ratios K_{33}^m/K_{11}^m estimated from the two experiments, 0.32 and 0.56, are quite different, leading to significantly different values of K_{33}^m, 3.9 and 6.4 pN, respectively. The inset shows the magnified parts of the curves in the vicinity of U_c, clearly demonstrating the difference in slope.

The fact that different cells were used for dielectric and optical measurements is also worth mentioning in this respect because these cells may differ in pretilt and anchoring energy. Our modeling, however, confirms that a 1° to 2° variation of the pretilt angle and quite large variations of anchoring

energy do not affect the *C(U)* curve to the level seen in the experiment. Therefore, we conclude that a defective texture is the main source of the discrepancy in the K_{33}^m values obtained by the two methods making the dielectric method less reliable. The optical method, in contrast, allows for selection of a very small and well-aligned uniform area for the measurement, and therefore is preferred for the calculation of the K_{33}^m values.

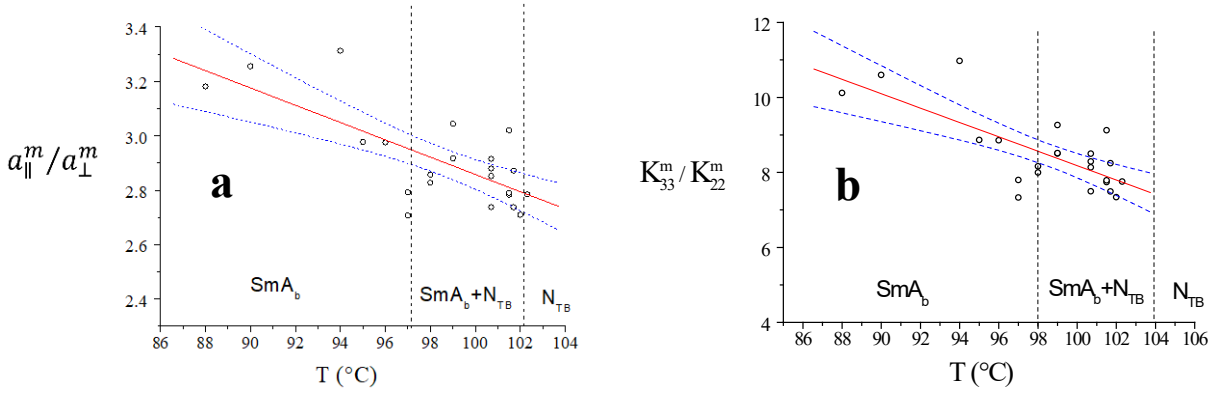

Figure 13. Temperature dependence of the measured axial ratio of the elliptical defect loops (**a**) and the ratio of the elastic constants (**b**) for twist and bend distortions of the **m**-director. The solid lines are linear interpolations of the data; the dashed lines show the upper and lower 95% confidence limits.

D. K_{22}^m elastic constant calculated from domain wall ellipticity

The temperature dependence of the axial ratio of the elliptical defect loops obtained by processing the video recordings (as described in Section II E) is presented in Fig. 13a.The temperature dependence of K_{22}^m (shown in Fig. 14) was calculated according to equation (4) from the ratios of K_{33}^m / K_{22}^m and K_{33}^m values obtained via the optical method (presented in Fig. 9, solid symbols). The summary of the obtained K_{ii}^m moduli is shown in Fig. 14.

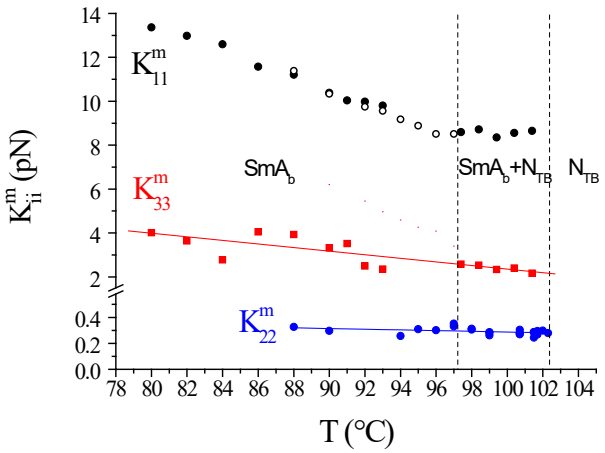

Figure 14. Temperature dependence of all three elastic moduli for the **m**-director distortion in the intercalated SmA_b phase of the BP12 mixture.

E. DISCUSSION

The similarity of the elliptical domain walls observed during the BFrTr and the ones occurring during the usual FrTr strikingly shows that the nematic **m**-director in the SmA_b phase behaves quite like the **n**-director of usual nematics. This means that the smectic positional order of the molecules does not affect the realignment ability of the **m**-director. This deep analogy between the realignment of **n** during the FrTr (studied in detail in Appendices A and B) and of **m** during the BFrTr underlies our calculations of K_{22}^m.

As evident from the elastic constant data (summarized in Figure 14), the temperature dependence of K_{11}^m and K_{33}^m in the SmA_b is qualitatively similar to that of common rod-like nematics. Both decrease with increasing temperature and are of the same order of magnitude but slightly smaller than those of 5CB [22]. However, one striking difference is that the ratio K_{11}^m / $K_{33}^m \approx 3$, whereas for common rod-like nematics $K_{33}^n \geq K_{11}^n$. As was discussed in Ref.[16], this behavior is typical for the nematics that also form a N_{TB} phase due to non-trivial bend elasticity. Moreover, in contrast to common rod-like nematics, in the

case of SmA_b, K_{11}^m and K_{33}^m are associated with the rotation of the molecule about its long axis [16], which requires less energy than the rotation about a short molecular axis .

Another surprising difference with common nematics is that the K_{22}^m constant is ten times smaller than K_{33}^m (and about 30 times smaller than K_{11}^m). Moreover, it is also almost one order of magnitude smaller than K_{22} of usual nematics like 5CB. Qualitatively, this behavior can be explained by the anticlinic orientation of the monomers in adjacent smectic layers of the intercalated SmA_b phase, which makes the nematic-like contribution to K_{22}^m negligible. The residual twist elasticity in the intercalated SmA_b phase should then only be attributed to the twist elasticity of the central spacer of the BNA-76 dimers, which is likely small due to the large number of possible conformations.

IV. CONCLUSIONS

By combining different experimental techniques, we measured all the principal dielectric, optic, and elastic constants and their temperature dependences in both the intercalated SmA_b phase and the SmA_b - N_{TB} biphasic coexistence range of the BP12 mixture. The measurement and subsequent modeling of the sample capacitance versus applied voltage curves allowed us to obtain the dielectric constants and elastic moduli K_{11}^m and K_{33}^m in the SmA_b. The measurement and modeling of the optical retardation of the sample as a function of applied voltage allowed us to obtain the refraction indices and the elastic moduli K_{11}^m and K_{33}^m in the SmA_b domains in both the monophasic SmA_b and the SmA_b - N_{TB} biphasic coexistence range. The analysis of the defect loops formed during the BFrTr of the **m**-director, coupled with a theoretical model that exploits the similarity with the FrTr in ordinary nematics, allowed us to also calculate K_{22}^m. Although the K_{11}^m and K_{33}^m elastic constants are of the same order of magnitude as the elastic constants of common rod-like nematics, K_{22}^m is abnormally small, about a tenth of the typical value of K_{22} for ordinary nematics. These remarkable features of the nematic-type elasticity of the **m**-director may in fact be typical of the intercalated SmA_b phase of bent-shaped dimers. In a follow-up paper, we will present a simple theoretical model for the estimation of the nematic-like elastic constants K_{ii}^m in the intercalated SmA_b phase of liquid-crystalline compounds of this kind.

The rather low values of K_{11}^m and K_{33}^m in the SmA_b phase, which is more typical of a nematic than of a smectic, are important for applications because relatively low voltages can be used for switching the device despite its operation in a smectic phase. Moreover, the very low rotational viscosity involved in

the BFrTr leads to response times that are about thirty times shorter than the typical ones for the FrTr [16]. The combination of these advantages suggests that the BFrTr of the **m**-director could find applications in non-display electro-optic devices that require fast switching.

Acknowledgements

A. K., I. Dokli, and A. L. thank the Croatian Science Foundation (Grant No. IP-2019-04-7978) and Ruđer Bošković Institute for financial support. This work was supported by the Agence Nationale pour la Recherche ANR (France) through Grant BESTNEMATICS, No. ANR-15-CE24-0012, by the French-Croatian bilateral program COGITO, and by the Université de Picardie Jules Verne, Amiens, France. This research was supported by the Hu Foundation, California State University, Sacramento.

Appendix A: Director distribution and elastic energy in a nematic monodomain during the electric-field-induced Fréedericksz transition

Before examining the shape of the wall separating two nematic domains with opposite signs of the tilt angle ψ (Fig. 4), let's first consider the energy stored in each individual monodomain when a usual nematic undergoes a Fréedericksz transition. Inside such a domain, the director distribution is uniform and is characterized by a splay-bend elastic deformation subject to zero pretilt at the LC layer boundaries. On both surfaces the director is oriented along the **x**-axis (see Fig. A1). The electric field is applied along the cell normal, **z**. When the applied voltage is larger than the FrTr threshold, $U > U_c$, the director tilts at an angle $\psi = \psi(z)$ but remains in the **xz**-plane:

$$\mathbf{n}(z) = (cos\ \psi(z),\ 0,\ sin\ \psi(z)\ ) \tag{A1}$$

The tilt angle reaches its maximum value, $\psi_m = \psi(d/2)$, in the middle of the LC layer and we assume that the applied voltage is small enough to satisfy the condition $\psi_m^2 << 1$.

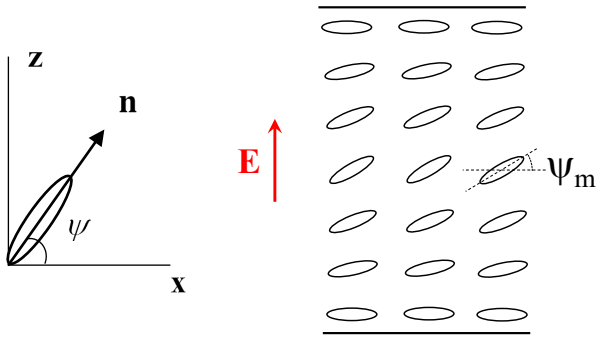

Figure A1. Single nematic monodomain undergoing a FrTr. (The director **n** is confined in a vertical plane.)

In the presence of the external electric field, the free energy of the LC per unit volume is:

$$f^n = \frac{1}{2}\left[K_{11}\big(\mathbf{n}(\boldsymbol{\nabla}\cdot\mathbf{n})\big)^2 + K_{22}\big(\mathbf{n}\cdot(\boldsymbol{\nabla}\times\mathbf{n})\big)^2 + K_{33}\big(\mathbf{n}\times(\boldsymbol{\nabla}\times\mathbf{n})\big)^2 + \boldsymbol{D}\cdot\boldsymbol{E}\right]. \tag{A2}$$

In our case, it takes the following form:

$$f = \frac{1}{2}\left[K_{11}cos^2\psi\left(\frac{\partial\psi}{\partial z}\right)^2 + K_{33}sin^2\psi\left(\frac{\partial\psi}{\partial z}\right)^2 + \frac{D^2}{\varepsilon_0[\varepsilon_\perp+\Delta\varepsilon sin^2\psi]}\right], \tag{A3}$$

Introducing the notations $\kappa = \frac{K_{33}-K_{11}}{K_{11}}$ and $\omega = \frac{\Delta\varepsilon sin^2\psi}{\varepsilon_\perp} << 1$ we have:

$$f = \frac{1}{2}K_{11}\left\{(1+\kappa sin^2\psi)\left(\frac{\partial\psi}{\partial z}\right)^2 + \frac{\varepsilon_0\varepsilon_\perp {E_0}^2}{K_{11}}\frac{1}{1+\omega}\right\}. \quad \text{(A4)}$$

Here, $E_0 = \frac{D}{\varepsilon_0\varepsilon_\perp} = const$, due to $D_z = D = const$. Since $\omega \ll 1$, the free energy density becomes:

$$f \approx \frac{1}{2}K_{11}\left[(1+\kappa sin^2\psi)\left(\frac{\partial\psi}{\partial z}\right)^2 + \frac{\varepsilon_0\varepsilon_\perp {E_0}^2}{K_{11}}(1-\omega+\omega^2)\right] =$$

$$= \frac{1}{2}K_{11}\left[(1+\kappa sin^2\psi)\left(\frac{\partial\psi}{\partial z}\right)^2 - \frac{\varepsilon_0\Delta\varepsilon {E_0}^2}{K_{11}}\, sin^2\psi\left(1-\frac{\Delta\varepsilon sin^2\psi}{\varepsilon_\perp}\right)\right]. \quad \text{(A5)}$$

Inside the domain, ψ is small, and since $\psi\,(0) = \psi\,(d) = 0$ at the boundaries, the function $\psi(z)$ is symmetric. It reaches its maximum amplitude at the middle of the cell: $\psi_m = \psi(d/2)$ and can be approximated by $\psi(z) = \psi_m\, sin\left(\frac{\pi z}{d}\right)$ that satisfies all these conditions. Substituting ψ by this function in Eq. (A5) and using $sin^2\psi \approx \psi^2 - \frac{1}{3}\psi^4$, we obtain the free energy per unit volume averaged over the thickness of the LC layer, $\bar{f}$:

$$\bar{f} = \frac{1}{d}\int_0^d f dz = \frac{1}{2}K_{11}\left\{\frac{1}{2}\left(\frac{\pi}{d}\right)^2\psi_m^2 + \frac{1}{8}\kappa\left(\frac{\pi}{d}\right)^2\psi_m^4 - \frac{\varepsilon_0\Delta\varepsilon {E_0}^2}{K_{11}}\left[\frac{1}{2}\psi_m^2 - \frac{3}{8}\psi_m^4\left(\frac{1}{3}+\frac{\Delta\varepsilon}{\varepsilon_\perp}\right)\right]\right\}. \quad \text{(A6)}$$

If ψ_m is small, then $\bar{f} \approx \frac{1}{4}K_{11}\psi_m^2\left\{\left(\frac{\pi}{d}\right)^2 - \frac{\varepsilon_0\Delta\varepsilon {E_0}^2}{K_{11}}\right\} \geq 0$. We then introduce a critical field E_c (the field at which the Fréedericksz threshold takes place):

$$E_c = \frac{U_c}{d} = \frac{\pi}{d}\sqrt{\frac{K_{11}}{\varepsilon_0\Delta\varepsilon}} \text{ so that } \left(\frac{\pi}{d}\right)^2 = \frac{E_c^2}{K_{11}}\varepsilon_0\Delta\varepsilon\,.$$

This transforms Eq. (A6) into:

$$\bar{f} = \frac{1}{4}\varepsilon_0\Delta\varepsilon\left\{\psi_m^2\left(E_c^2 - {E_0}^2\right) + \frac{1}{4}\psi_m^4\left[\kappa E_c^2 + \left(1+\frac{3\Delta\varepsilon}{\varepsilon_\perp}\right){E_0}^2\right]\right\} \quad \text{(A7)}$$

Minimization with respect to ψ_m results in:

$$\psi_m^2 = \frac{2({E_0}^2 - {E_c}^2)}{\kappa E_c^2 + \left(1+\frac{3\Delta\varepsilon}{\varepsilon_\perp}\right){E_0}^2}\,, \quad \text{(A8)}$$

which is valid for small κ and $\Delta\varepsilon/\varepsilon_\perp$ ratio.

Let's now calculate the voltage U as a function of the integration constant E_0 defined above.

By using $D_z=D=\varepsilon_o(\varepsilon_\perp+\Delta\varepsilon\sin^2\psi)E(z)$, we obtain $E(z)=\frac{E_0}{1+\frac{\Delta\varepsilon}{\varepsilon_\perp}sin^2\psi}$, and then:

$$U=\int_0^d E(z)dz\approx E_0\int_0^d\frac{1}{1+\frac{\Delta\varepsilon}{\varepsilon_\perp}\psi^2\left(1-\frac{1}{3}\psi^2\right)}dz. \quad \text{(A9)}$$

Let's now approximate U further, recognizing that the quantity $\alpha=\frac{\Delta\varepsilon}{\varepsilon_\perp}\psi^2\left(1-\frac{1}{3}\psi^2\right)$ is small. Then, up to terms of the order ψ_m^4 we obtain:

$$U\approx E_0\int_0^d\left\{1-\frac{\Delta\varepsilon}{\varepsilon_\perp}\psi_m^2\,sin^2\left(\frac{\pi z}{d}\right)\left[1-\frac{1}{3}\psi_m^2\,sin^2\left(\frac{\pi z}{d}\right)\right]+\left(\frac{\Delta\varepsilon}{\varepsilon_\perp}\right)^2\psi_m^4\,sin^4\left(\frac{\pi z}{d}\right)\right\}dz, \quad \text{(A10)}$$

which results in:

$$U=E_0d\left[1-\frac{1}{2}\frac{\Delta\varepsilon}{\varepsilon_\perp}\psi_m^2+\frac{1}{8}\frac{\Delta\varepsilon}{\varepsilon_\perp}\left(1+3\frac{\Delta\varepsilon}{\varepsilon_\perp}\right)\psi_m^4\right]. \quad \text{(A11)}$$

For $\psi^2\ll 1$, both U and ψ_m^2 are simple functions of the integration constant E_0. As the component of the dielectric permittivity tensor ε_{zz} and the optical anisotropy Δn are both functions of ψ^2, they can also be obtained as functions of E_0. (The same approach was used for fitting of the $C(U)$ curves.)

Appendix B: Excess energy of the domain wall between twin domains and shape of the loop around a domain

After establishing the energy density function of a nematic monodomain (Appendix A), we now calculate the excess energy of a domain wall that separates two monodomains with opposite director tilts. Let's first calculate the energy stored in the domain wall. Since the wall encircles the domain, its orientation with respect to the director varies. Therefore, an important twist distortion is present across the wall and needs to be considered. Let the field be applied along the **z**-axis, resulting in the formation of twin domains separated by an infinitely long straight wall placed at $x = 0$ and parallel to the **y**-axis. On the two cell surfaces the imposed orientation of the director **n** is in the **xy**-plane and makes an angle φ with the **x**-axis (Figure B1). In this geometry, the director is:

$$\mathbf{n} = (cos\varphi cos\psi, sin\varphi cos\psi, sin\psi) \quad \text{(B1)}$$

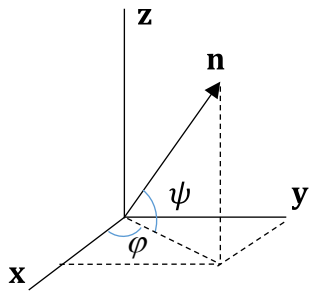

Figure B1: Director geometry and notations used in the calculations

Under the field, **n** rotates in a vertical plane and the angle φ remains constant and independent of the position. On the contrary, inside the domain wall $\psi = \psi(x, z)$ and, in the middle of the wall, ψ vanishes: $\psi(0, z) = 0$, while far from the wall (deep inside the monodomain) ψ depends only on z, as shown in Appendix A.

The free energy density is:

$$f = \frac{1}{2}\Big\{K_{11}\left(-cos\varphi sin\psi\,\frac{\partial\psi}{\partial x} + cos\psi\,\frac{\partial\psi}{\partial z}\right)^2 + K_{22}\,sin^2\varphi\left(\frac{\partial\psi}{\partial x}\right)^2 + K_{33}\Big[\,sin^2\psi\left(\frac{\partial\psi}{\partial z}\right)^2 +$$

$$cos\varphi\;\,sin(2\psi)\frac{\partial\psi}{\partial z}\frac{\partial\psi}{\partial x} + cos^2\psi\,cos^2\varphi\left(\frac{\partial\psi}{\partial x}\right)^2\Big]\Big\} + \frac{\boldsymbol{D}\cdot\boldsymbol{E}}{2}. \qquad \text{(B2)}$$

The total energy can be minimized using a separation of the variables and an ansatz function invoked by the 1D-solution in Appendix A:

$$\psi(x,z) = \psi_m(E_0)\,X(x)\,Z(z) = \psi_m\,X(x)\,sin\left(\frac{\pi z}{d}\right), \qquad \text{(B3)}$$

where $X(x) \to \pm 1$ at $\pm\infty$ and $X(0) = 0$. Assuming that the wall thickness is proportional to $\frac{1}{\psi_m}$ and $\frac{\partial X}{\partial x} \sim \psi_m$[24], after omitting the terms of order higher than ψ_m^4 and disregarding the terms containing $cos\left(\frac{\pi z}{d}\right)$ (since they integrate to zero over the thickness of the cell), but keeping the terms containing $cos^2\left(\frac{\pi z}{d}\right)$, the approximate free energy density reads:

$$f = \frac{1}{2}K_{11}\Big\{\left(\frac{\pi}{d}\right)^2\psi_m^2\,cos^2\left(\frac{\pi z}{d}\right)\,[X(x)]^2 - \left(\frac{\pi}{d}\right)^2\psi_m^4\,sin^2\left(\frac{\pi z}{d}\right)cos^2\left(\frac{\pi z}{d}\right)\,[X(x)]^4 +$$

$$\frac{K_{22}}{K_{11}}\,sin^2\varphi\,\psi_m^2 sin^2\left(\frac{\pi z}{d}\right)\,[X'(x)]^2 + \frac{K_{33}}{K_{11}}\Big[\left(\frac{\pi}{d}\right)^2\psi_m^4\,sin^2\left(\frac{\pi z}{d}\right)cos^2\left(\frac{\pi z}{d}\right)[X(x)]^4 +$$

$$\psi_m^2\,cos^2\varphi\,sin^2\left(\frac{\pi z}{d}\right)\,[X'(x)]^2\Big] - \frac{\varepsilon_0\Delta\varepsilon{E_0}^2}{K_{11}}\Big[\psi_m^2\,sin^2\left(\frac{\pi z}{d}\right)[X(x)]^2 - \left(\frac{1}{3}+\frac{\Delta\varepsilon}{\varepsilon_\perp}\right)\psi_m^4\,sin^4\left(\frac{\pi z}{d}\right)[X(x)]^4\Big]\Big\}$$

(B4)

Averaging over the thickness of the cell results in:

$$\langle f\rangle_z = \frac{1}{d}\int_0^d f(z)dz = \frac{1}{4}K_{11}\left\{\left(\frac{\pi}{d}\right)^2\psi_m^2\,[X(x)]^2 + \chi_2\,\psi_m^2\,sin^2\varphi\,[X'(x)]^2 + \kappa\frac{1}{4}\left(\frac{\pi}{d}\right)^2\psi_m^4[X(x)]^4 +\right.$$

$$\left.\chi_3\psi_m^2 cos^2\varphi\,[X'(x)]^2 - \frac{1}{\xi^2}\left[\psi_m^2\,[X(x)]^2 - \frac{3}{4}\left(\frac{1}{3}+\frac{\Delta\varepsilon}{\varepsilon_\perp}\right)\psi_m^4\,[X(x)]^4\right]\right\}. \qquad \text{(B5)}$$

where we introduced $\chi_2 = \frac{K_{22}}{K_{11}}$, $\chi_3 = \frac{K_{33}}{K_{11}}$, and $\frac{1}{\xi^2} = \frac{\varepsilon_0\Delta\varepsilon{E_0}^2}{K_{11}}$. Finally, Eq. (B5) takes the following form:

$$\langle f\rangle_z = \frac{1}{4}K_{11}\left(\frac{\pi}{d}\right)^2\left\{\left[1-\left(\frac{d}{\pi\xi}\right)^2\right]\psi_m^2\left(X(x)\right)^2 + \left(\frac{d}{\pi}\right)^2(\chi_2\,sin^2\varphi + \chi_3 cos^2\varphi)\psi_m^2\left(X'(x)\right)^2 +\right.$$

$$\left.\frac{1}{4}\left[\kappa + \left(\frac{d}{\pi\xi}\right)^2\left(1+\frac{3\Delta\varepsilon}{\varepsilon_\perp}\right)\right]\psi_m^4\left(X(x)\right)^4\right\} \qquad \text{(B6)}$$

We now introduce $v = \frac{d}{\pi\xi} = \frac{\xi_c}{\xi} = \frac{E_0}{E_c}$, $\Phi^2 = \chi_2\, sin^2\varphi + \chi_3 cos^2\varphi$, and $A = \frac{1}{\kappa}\left(1 + \frac{3\Delta\varepsilon}{\varepsilon_\perp}\right)$, and use the relation $\psi_m^2 = \frac{2\left(E_0^2 - E_c^2\right)}{\kappa\left(E_c^2 + AE_0^2\right)} = \frac{2}{\kappa}\,\frac{v^2-1}{1+Av^2}$ from Eq. (A8) which results in:

$$\langle f\rangle_z = \frac{1}{4\xi_c^2} K_{11}\left\{(1-v^2)\psi_m^2\,[X(x)]^2 + \xi_c^2\Phi^2\psi_m^2\,[X'(x)]^2 + \frac{1}{4}\kappa[1+Av^2]\psi_m^4\,[X(x)]^4\right\}. \qquad \text{(B7)}$$

To find the shape of the domain wall, the functional $\int\langle f\rangle_z dx$ needs to be minimized. As in our case $\langle f\rangle_z$ does not depend explicitly on x, we employ the Beltrami identity, $\langle f\rangle_z - X'(x)\frac{\partial\langle f\rangle_z}{\partial X\prime(x)} = const.$:

$$\frac{1}{4\xi_c^2} K_{11}\left\{(1-v^2)\psi_m^2\,[X(x)]^2 - \xi_c^2\Phi^2\psi_m^2\,[X'(x)]^2 + \frac{1}{4}\kappa(1+Av^2)\psi_m^4\,[X(x)]^4\right\} = const. \qquad \text{(B8)}$$

When $x \to \pm\infty$, far from the wall, $X'(x) \to 0$ and $X(x) \to 1$, thus the constant in Eq. (B8) is equal to $\frac{1}{4\xi_c^2} K_{11}\left\{(1-v^2)\psi_m^2 + \frac{1}{4}\kappa[1+Av^2]\psi_m^4\right\}$, and we obtain the following differential equation for $X(x)$:

$$X'(x) = \frac{\sqrt{v^2-1}}{\sqrt{2}\xi_c\Phi}\left[1 - \left(X(x)\right)^2\right]. \qquad \text{(B9)}$$

We seek the solution of this equation in the form $X(x) = \tanh ax$ and find:

$$X(x) = \tanh\left[\frac{\pi\sqrt{v^2-1}}{\sqrt{2}\Phi d}x\right], \qquad \text{(B10)}$$

and, finally,

$$X(x) = \tanh\left[\frac{\pi\psi_m}{2\Phi d}\sqrt{\kappa + \left(1+\frac{3\Delta\varepsilon}{\varepsilon_\perp}\right)\left(\frac{d}{\pi\xi}\right)^2}\,x\right]. \qquad \text{(B11)}$$

Let's now calculate the excess energy of the domain wall by taking the difference between its energy and the energy of the uniform domain. Inside the uniform domain $X(x) = 1$ and $X'(x) = 0$. From Eq. (B7), the average free energy density inside the monodomain is:

$$\langle f\rangle_z^0 = \frac{1}{d}\int f_{\,\Big|\,\substack{X(x)=1\\X'(x)=0}}\, dz = \frac{1}{4\xi_c^2} K_{11}\left\{(1-v^2)\psi_m^2 + \frac{1}{4}\kappa[1+Av^2]\psi_m^4\right\} = \frac{1}{8\xi_c^2} K_{11}(1-v^2)\psi_m^2, \qquad \text{(B12)}$$

and the excess energy of the domain wall becomes:

$$\Delta F = d\int_{-\infty}^{\infty}(\langle f\rangle_z - \langle f\rangle_z^0)\,dx = \frac{1}{4\xi_c^2} K_{11} d\int_{-\infty}^{\infty}\left\{(v^2-1)\frac{\psi_m^2}{2}\left(\left(X(x)\right)^2 - 1\right)^2 + \xi_c^2\Phi^2\psi_m^2\left(X'(x)\right)^2\right\}dx \qquad \text{(B13)}$$

Substituting the solutions for ψ_m^2 and $X(x)$ from Eqs. (A8) and (B10) and integrating, we obtain:

$$\Delta F = B\sqrt{\frac{K_2}{K_1}\sin^2\varphi + \frac{K_3}{K_1}\cos^2\varphi}, \tag{B14}$$

where the coefficient

$$B = \frac{2\sqrt{2}K_{11}\pi}{3\kappa}\frac{\left(\left(\frac{d}{\pi\xi}\right)^2 - 1\right)^{3/2}}{1+\frac{1}{\kappa}\left(1+\frac{3\Delta\varepsilon}{\varepsilon_\perp}\right)\left(\frac{d}{\pi\xi}\right)^2} \tag{B15}$$

is a function of the applied voltage but is independent of the wall orientation.

When one kind of domain is surrounded by a domain with the opposite sign of the tilt, the shape of the wall loop separating the twin-domains is defined by the anisotropy of the excess energy. The anisotropy of the expression in Eq. (B14) is the same as in Ref. 24 (with a different coefficient B because $K_{11} \neq K_{33}$ and the ratio $\Delta\varepsilon/\varepsilon_\perp$ is finite). Therefore, we expect that the equilibrium shape of the loop will be again, as in Ref. 24, an ellipse with axial ratio given by

$$a_\parallel / a_\perp = (K_{33}/K_{22})^{1/2}. \tag{B16}$$

(This is easily demonstrated by noting that the expression under the square root in Eq. (14) is a parametric equation of an ellipse with axial ratio $(K_{33}/K_{22})^{1/2}$; after transformation of the coordinate system by reducing the long axis of the ellipse by this ratio, the ellipse becomes a circle, which is obviously the shape that minimizes the loop energy at constant area of the domain.)

References

1. Frank FC. I. Liquid crystals. On the theory of liquid crystals. Faraday Discuss. 1958;25(0):19-28.
2. Fréedericksz V, Zolina V. Forces causing the orientation of an anisotropic liquid. Trans Faraday Soc. 1933;29:919-930.
3. de Gennes PG, Prost J. The Physics of Liquid Crystals: Clarendon, Oxford; 1994.
4. Dozov I. On the spontaneous symmetry breaking in the mesophases of achiral banana-shaped molecules. EPL (Europhysics Letters). 2001;56(2):247.
5. Cestari M, Diez-Berart S, Dunmur DA, Ferrarini A, de la Fuente MR, Jackson DJB, Lopez DO, Luckhurst GR, Perez-Jubindo MA, Richardson RM, Salud J, Timimi BA, Zimmermann H. Phase behavior and properties of the liquid-crystal dimer 1 ",7 "-bis(4-cyanobiphenyl-4 '- yl) heptane: A twist-bend nematic liquid crystal. Phys Rev E. 2011;84(3):031704.
6. Shamid SM, Dhakal S, Selinger JV. Statistical mechanics of bend flexoelectricity and the twist-bend phase in bent-core liquid crystals. Phys Rev E. 2013;87(5):052503.
7. Freiser MJ. Ordered states of a nematic liquid Phys Rev Lett. 1970;24(19):1041.
8. Yu LJ, Saupe A. Observation of a biaxial nematic phase in potassium laurate-1-decanol-water mixtures. Phys Rev Lett. 1980;45(12):1000-1003.
9. Luckhurst GR, Sluckin TJ, editors. Biaxial nematic liquid crystals: theory, simulation and experiment: Wiley; 2015.
10. Saupe A. Elastic and flow properties of biaxial nematics. J Chem Phys. 1981;75(10):5118-5124.
11. Govers E, Vertogen G. Elastic continuum theory of biaxial nematics. Phys Rev A. 1984;30(4):1998-2000.
12. Rapini A. Magnetic instabilities of a smectic-C. J Phys (Paris). 1972;33(2-3):237.
13. Mandle RJ, Goodby JW. A twist-bend nematic to an intercalated, anticlinic, biaxial phase transition in liquid crystal bimesogens. Soft Matter. 2016;12(5):1436-1443.
14. Hegmann T, Kain J, Diele S, Pelzl G, Tschierske C. Evidence for the existence of the McMillan phase in a binary system of a metallomesogen and 2,4,7-trinitrofluorenone. Angew Chem Int. 2001;40(5):887-890.
15. Eremin A, Diele S, Pelzl G, Nadasi H, Weissflog W, Salfetnikova J, Kresse H. Experimental evidence for an achiral orthogonal biaxial smectic phase without in-plane order exhibiting antiferroelectric switching behavior. Phys Rev E. 2001;64(5):051707.
16. Meyer C, Davidson P, Constantin D, Sergan V, Stoenescu D, Knezevic A, Dokli I, Lesac A, Dozov I. Freedericksz-Like Transition in a Biaxial Smectic-A Phase. Phys Rev X. 2021;11(3):031012.
17. Knežević A, Sapunar M, Buljan A, Dokli I, Hameršak Z, Kontrec D, Lesac A. Fine-tuning the effect of pi-pi interactions on the stability of the N-TB phase. Soft Matter. 2018;14(42):8466-8474.
18. Deuling HJ. Deformation of nematic liquid-crystals in an electric-field. Mol Cryst Liq Cryst. 1972;19(2):123-131.
19. Gruler H, Scheffer TJ, Meier G. Elastic-constants of nematic liquid-crystals .1. Theory of normal deformation. Zeitschrift Fur Naturforschung Part a-Astrophysik Physik Und Physikalische Chemie. 1972;A 27(6):966.
20. Morris SW, Palffy-Muhoray P, Balzarini DA. Measurements of the bend and splay elastic-constants of octylcyanobiphenyl. Mol Cryst Liq Cryst. 1986;139(3-4):263-280.
21. Uchida T, Takahashi Y. New method to determine elastic-constants of nematic liquid-crystal from C-V curve. Mol Cryst Liq Cryst. 1981;72(4):133-137.
22. Bogi A, Faetti S. Elastic, dielectric and optical constants of 4'-pentyl-4-cyanobiphenyl. Liq Cryst. 2001;28(5):729-739.

23. Meyer C, Blanc C, Luckhurst GR, Davidson P, Dozov I. Biaxiality-driven twist-bend to splay-bend nematic phase transition induced by an electric field. Sci Adv. 2020;6(36):eabb8212.
24. Brochard F. Motion of walls in a thin nematic film. J Phys (Paris). 1972;33(5-6):607.
25. Leger L. Static and dynamic behavior of walls in nematics above a Fredericks transition. Solid State Communications. 1972;11(11):1499.
26. Léger L. Walls in Nematics. Mol Cryst Liq Cryst. 1973;24(1-2):33-44.
27. Blinov LM. Structure and Properties of Liquid Crystals. Dordrecht Heidelberg London New York: Springer; 2011.